Electronic Supplementary Material (ESI) for Analyst.

Compositional assessment of bone by Raman spectroscopy

Mustafa Unal, Rafay Ahmed, Anita Mahadevan-Jansen, and Jeffry S. Nyman

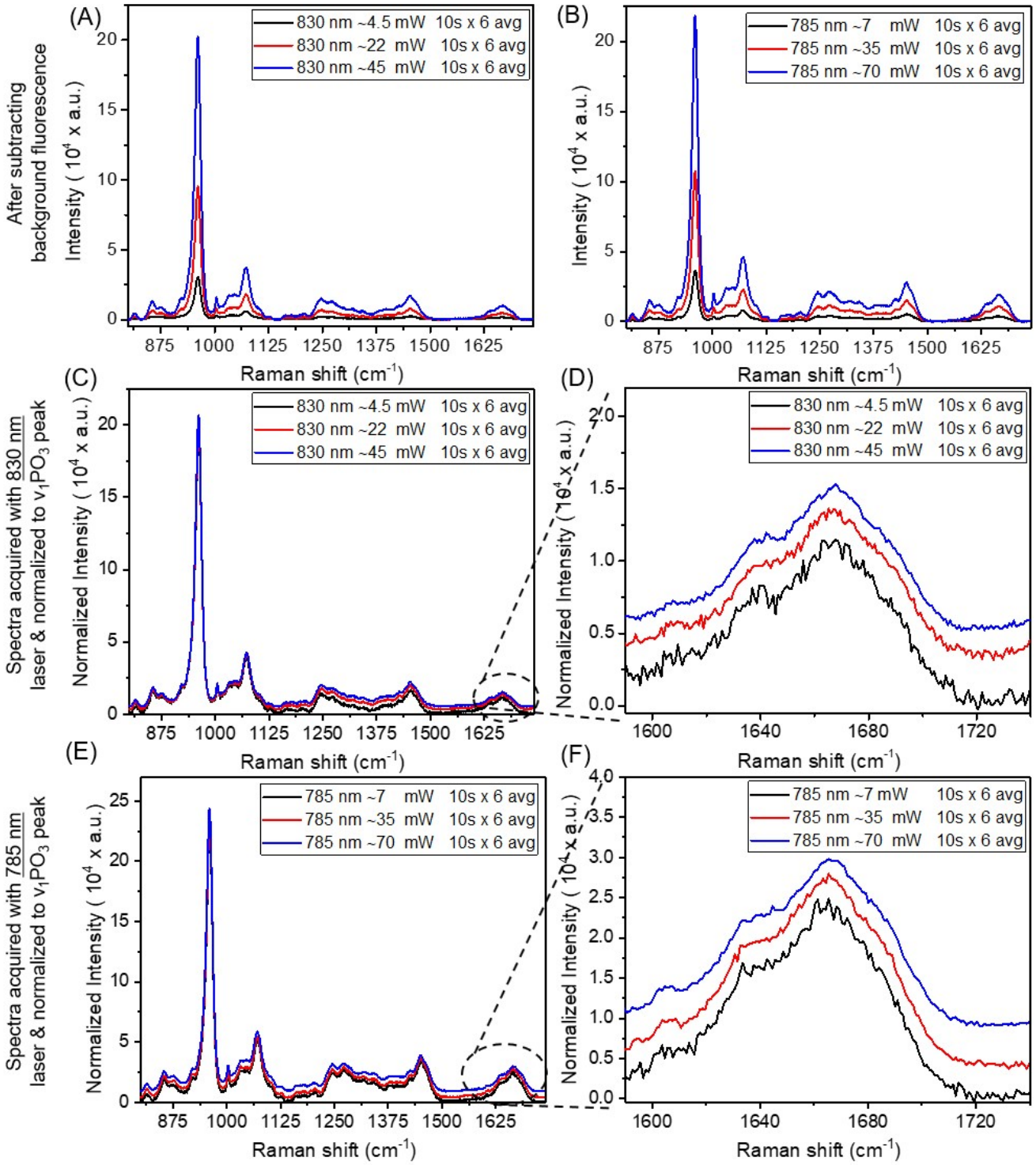

Figure S1: Effect of laser power on the Raman spectrum of human cortical bone. Regardless of whether the laser wavelength is 830 nm (A) or 785 nm (B), increasing the laser power improves the Raman signals and spectral quality. Raman spectra were collected from the same spot using three different laser power settings (4.5 mW to 45 mW or 7 mW to 70 mW) and the same integration time (10 s) and number of accumulations (average of 6). Increasing the power of 830 nm laser by 5 or 10 times increases the height of multiple peaks relative to the nu1 phosphate peak at 960 cm^{-1} (C) and improves the spectral quality (lower noise) of the amide I band (D). This is also the case when the spectra were collected using laser with a shorter wavelength (E, F).

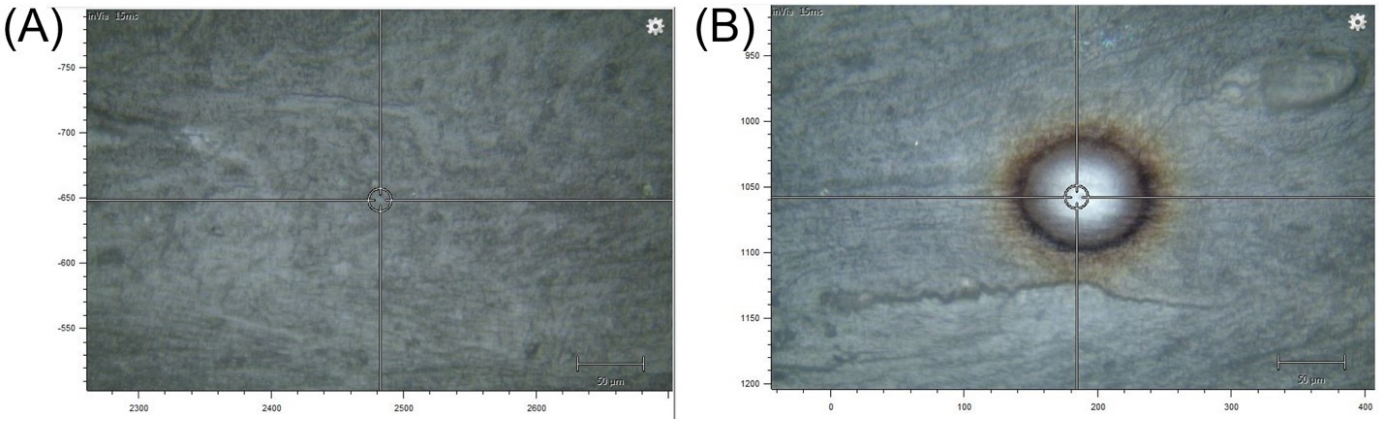

Figure S2: The appearance of a burn mark on human cortical bone. If the power of laser and the scan time is long enough to heat the bone tissue (A) above ~70 °C, a burn mark forms at the spot of the laser (B).

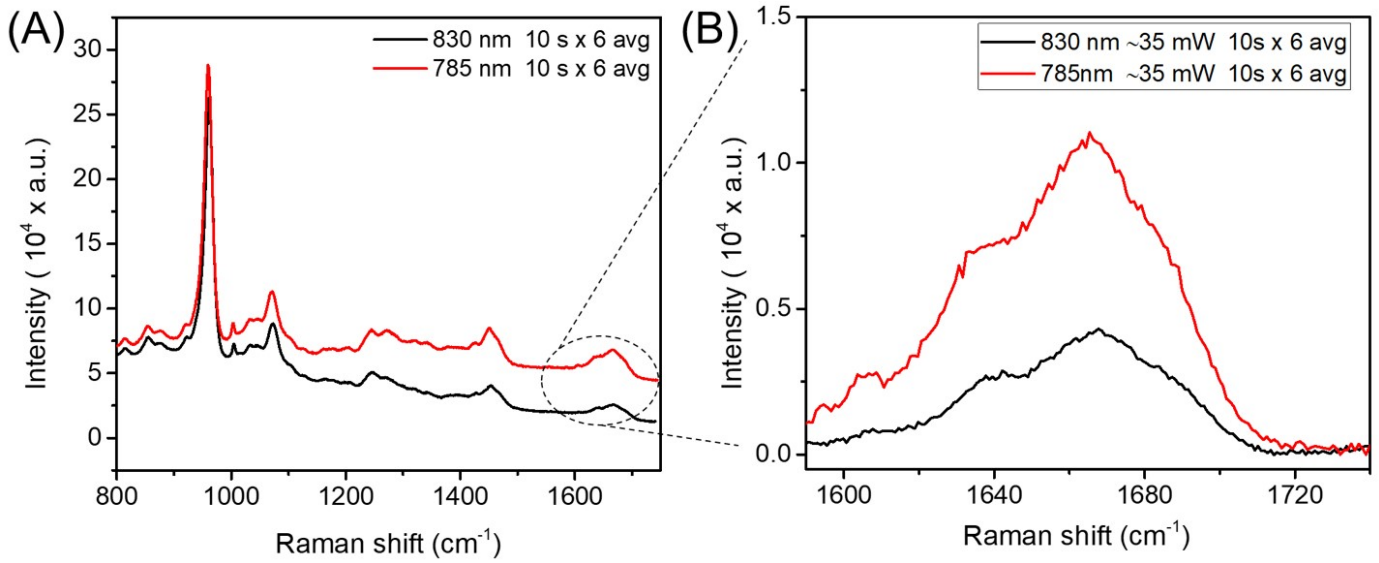

Figure. S3: Effect of laser wavelength on the Raman spectrum of human cortical bone. Raman spectra were collected from the same human bone specimen at the same spot using the same acquisition parameters (laser power and integration time x accumulation). While the 785 nm laser provides higher Raman signal intensities compared to the 830 nm laser, the fluorescence background is higher with lower laser wavelength (A). After baseline subtraction, a weak band such as amide I is more prominent for the 785 nm than for the 830 nm laser (B).

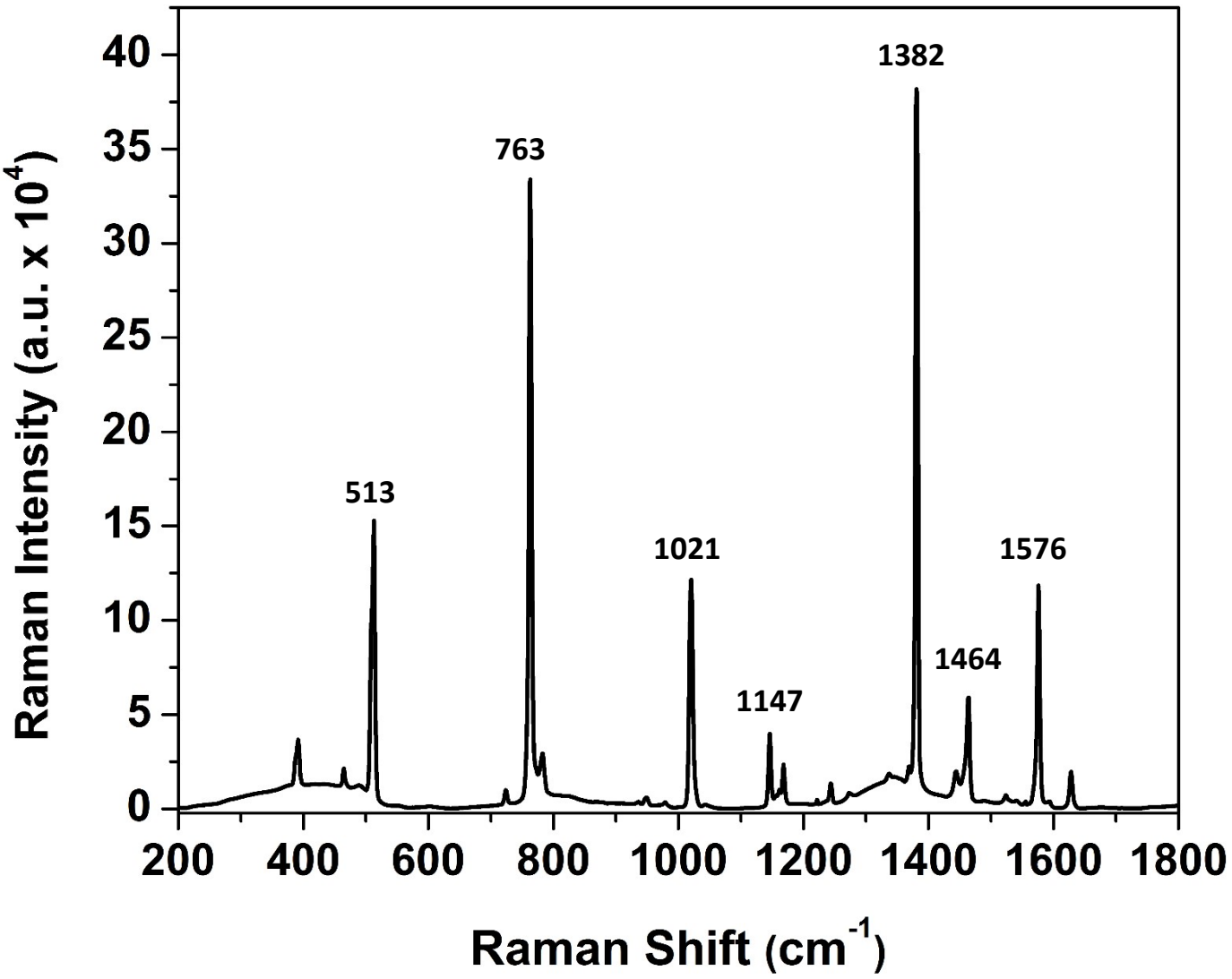

Figure S4: Raman spectrum of a standard material. A spectrum was acquired from naphthalene using a Renishaw inVia Raman microscope with 10 s exposure, 5 accumulations, and ~55 mW power (785 nm laser). When properly calibrated, the wavenumber position of each peak matches reported values.

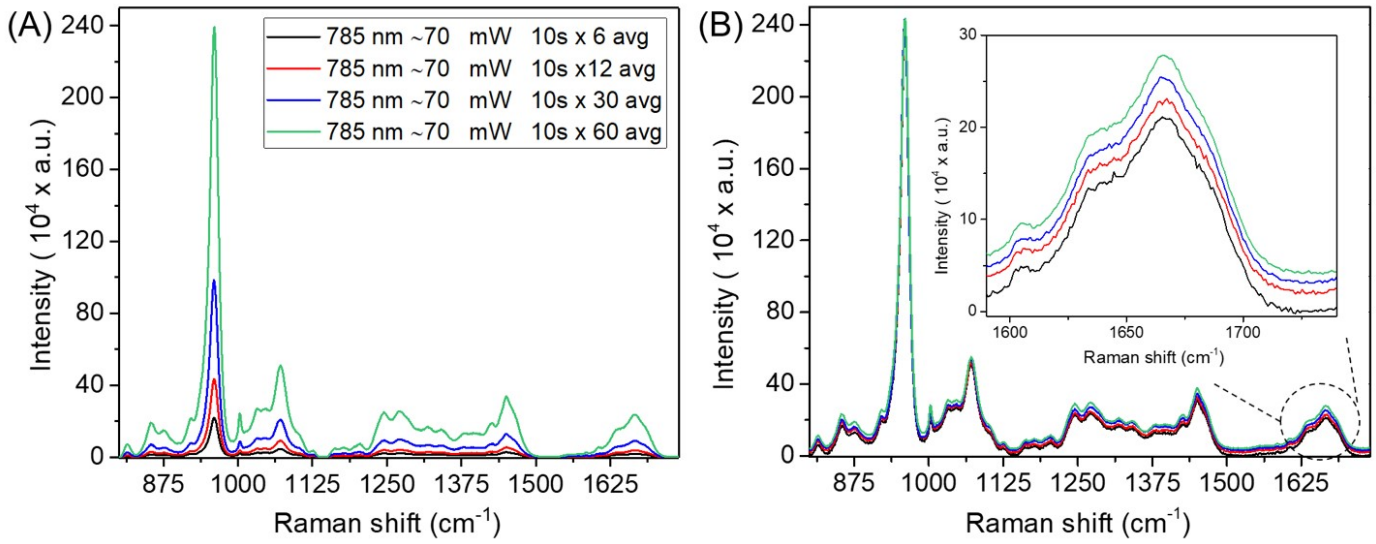

Figure S5: Effect of number of accumulations on the Raman spectrum of bone. Raman spectra were acquired from the same human cortical bone specimen using a 785 nm laser at 70 mW and integration time of 10 s. As the number of accumulations being averaged increases, the signal intensity of all Raman peaks increases (A). Upon normalizing the spectra, the apparent shot-noise decreases from 6 to 60 accumulations (B). Such a strategy to boost signal-to-noise ratio (SNR) adds time to the scan going from 1 min to 10 min.

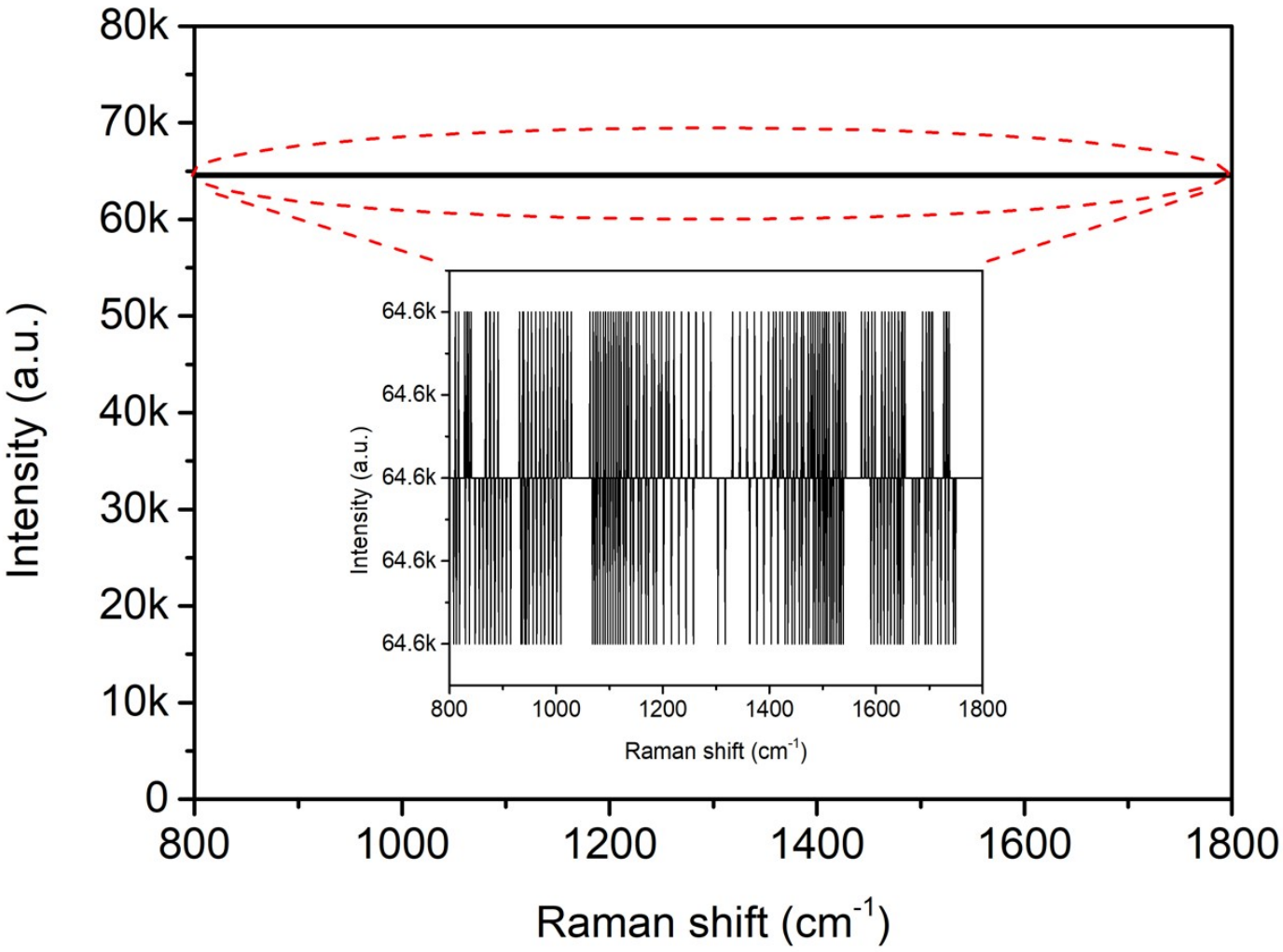

Figure S6: Saturation of the capacity of the detector that records a Raman spectrum. A high background fluorescence can easily overwhelm the weak Raman signal and cause the highly sensitive CCD detector to saturate. In such a situation, the obtained Raman spectrum appears as a straight line with very high signal counts. The characteristic pattern of the saturation (inset) indicates indistinguishable signals from the bone sample. To keep the CCD from saturating, lower laser power can be implemented as a first step. If that does not work, then different strategies such as bleaching the bone surface or photobleaching the bone specimen prior to the acquiring Raman spectrum can be considered.

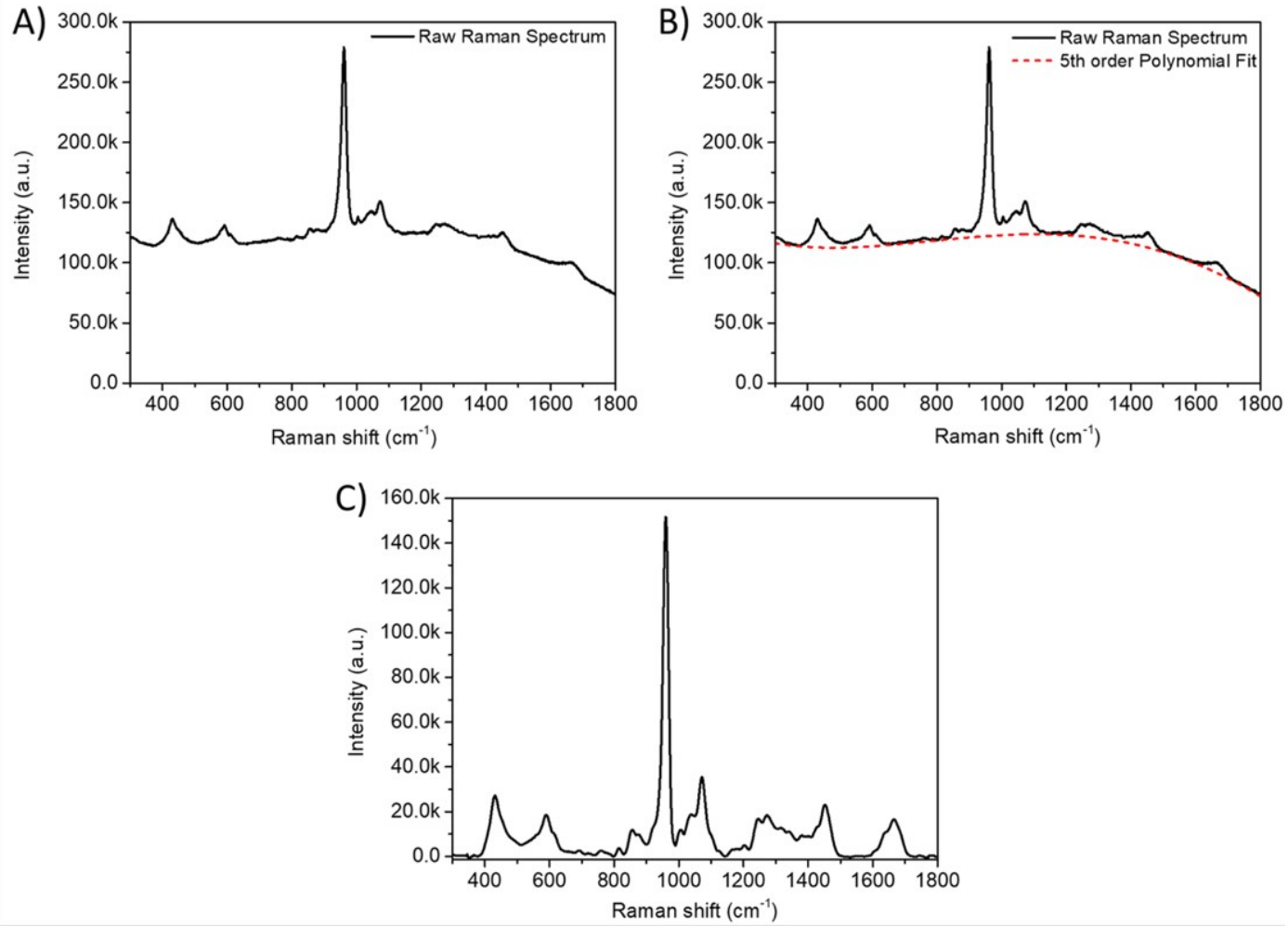

Figure S7: Subtraction of background fluorescence. Removing background fluorescence from a raw Raman spectrum of bone (A) typically involves fitting a polynomial curve to regions with low signal intensity (B) and subtracting the fitted baseline curve (red dash) from the raw spectrum to achieve a spectrum with minimal fluorescence (C).

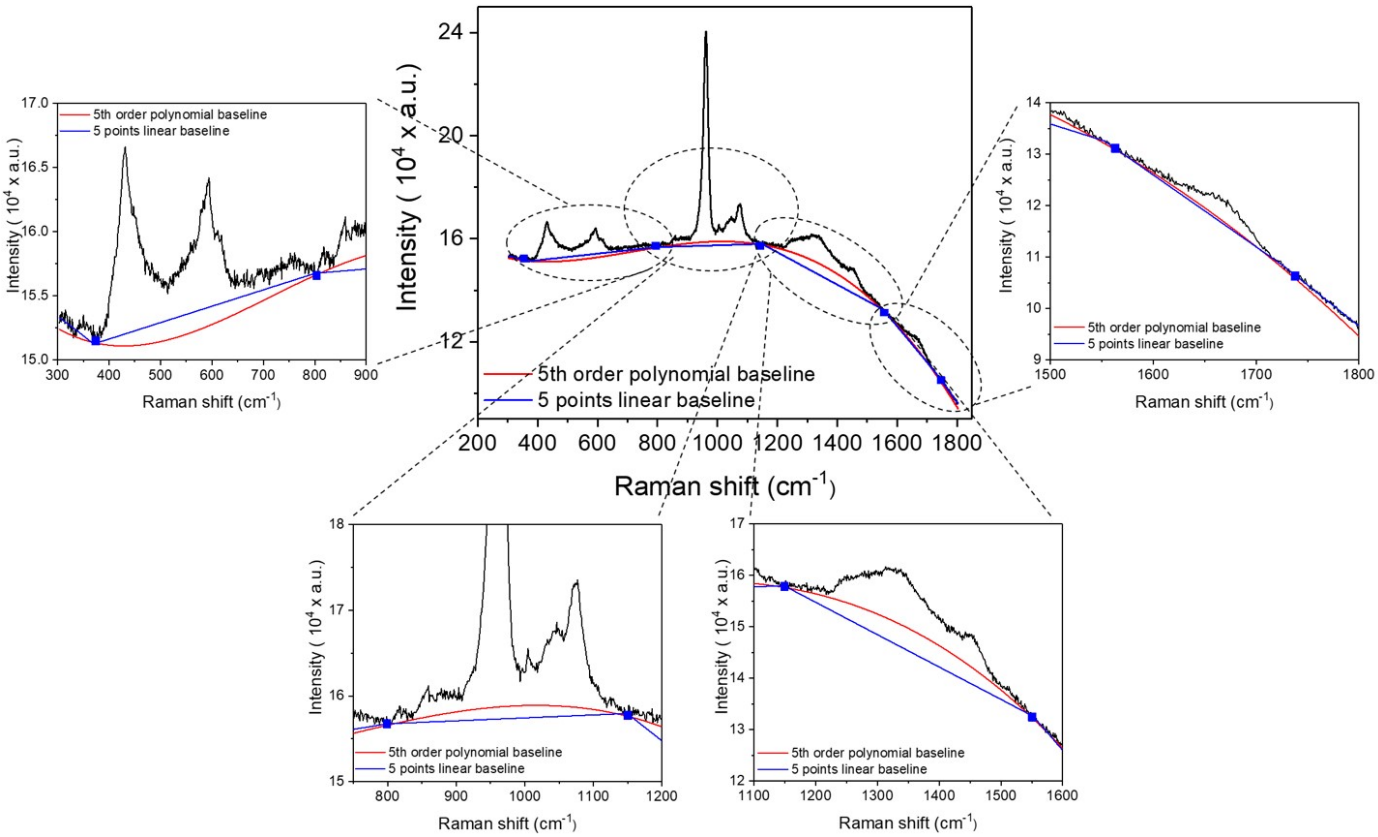

Figure S8: Selecting points along the Raman shift for baseline subtraction. In fitting a polynomial curve or a series of linear curves to the raw Raman spectrum of bone, points are selected in regions where signal intensity is low. Commercial software for spectroscopic analysis provides automated routines for selecting the points and fitting the curve(s).

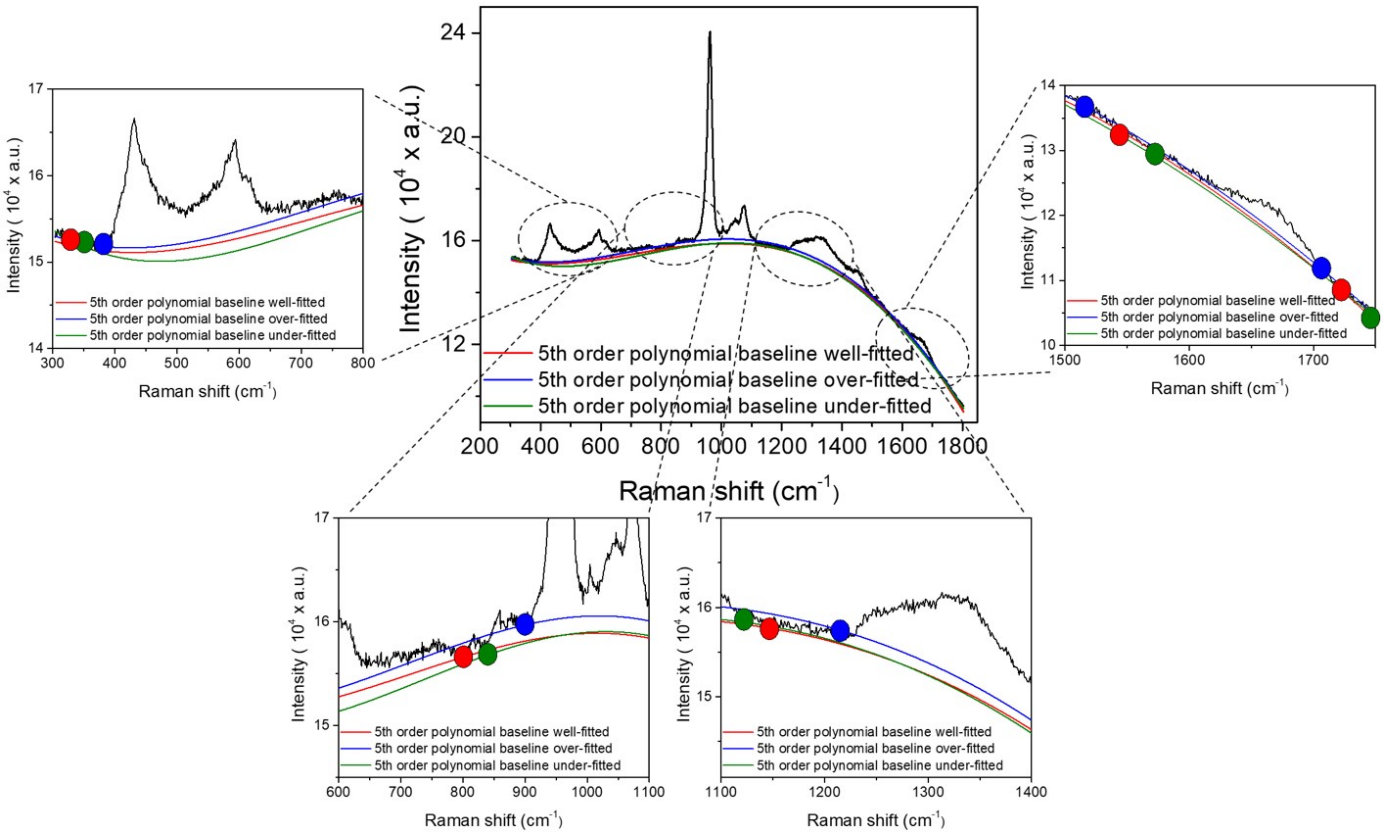

Figure S9: Effect of the spectral point selection on baseline fitting. Changing the location of 5 spectral points where the polynomial curve passes through the base from regions of the Raman shift with no obvious Raman peaks to regions that are close to Raman peaks results in the polynomial baseline that is either over-fitted or under-fitted. Red circles indicate the spectral points which provided a well-fitted polynomial baseline while green and blue circles indicate the spectral points resulting in an under-fitted and over-fitted polynomial baseline, respectively.

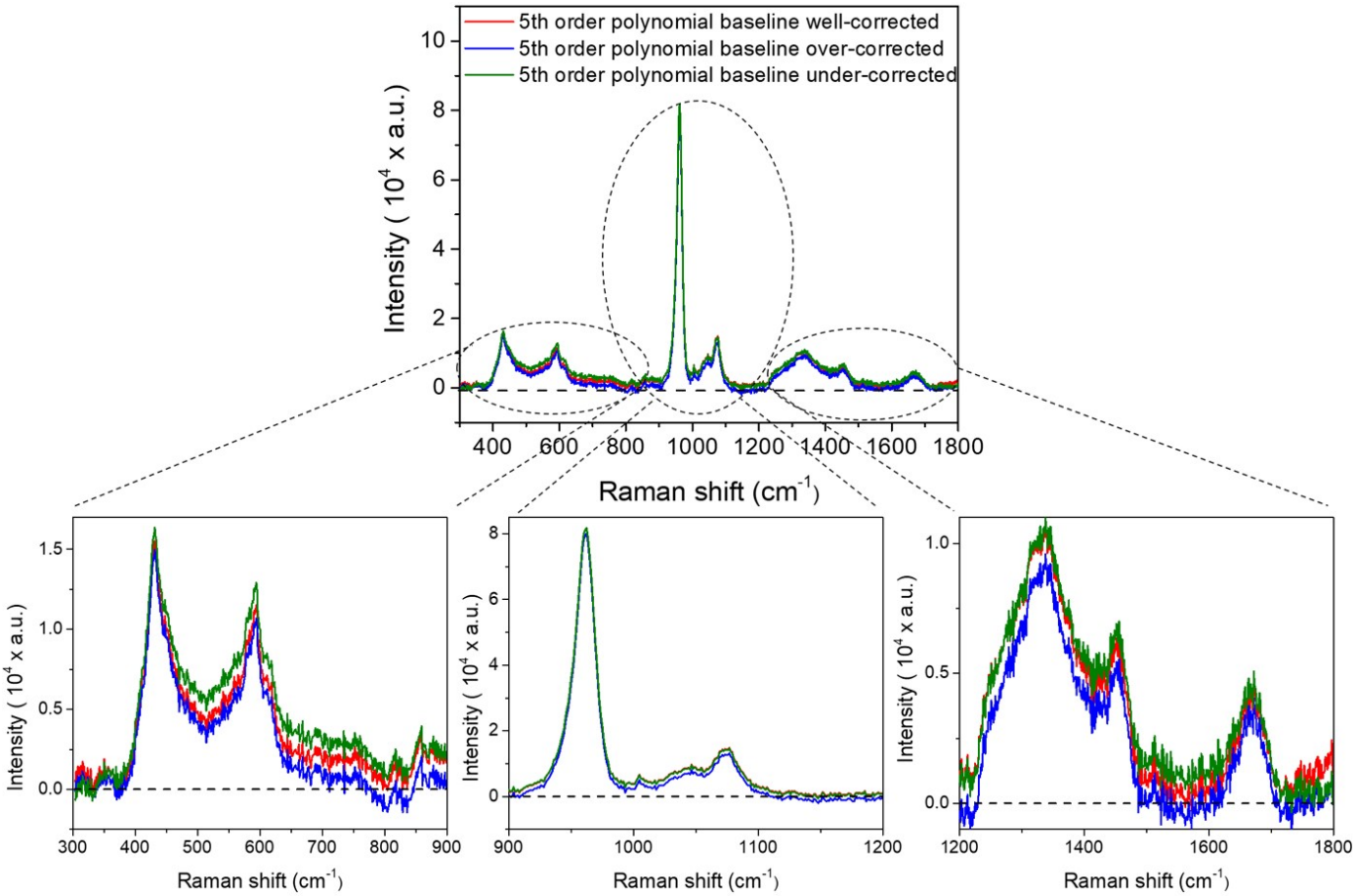

Figure S10: Effect of under- and over-correcting for background fluorescence subtraction. While subtraction of under-fitted baseline from the spectrum causes artificially elevated intensities in some parts of the spectrum, subtraction of over-fitted baseline from the spectrum causes negative intensities in parts of the spectrum. Therefore, following a baseline subtraction, we recommend checking the Raman spectra visually for negative or exaggeratedly high intensity values.

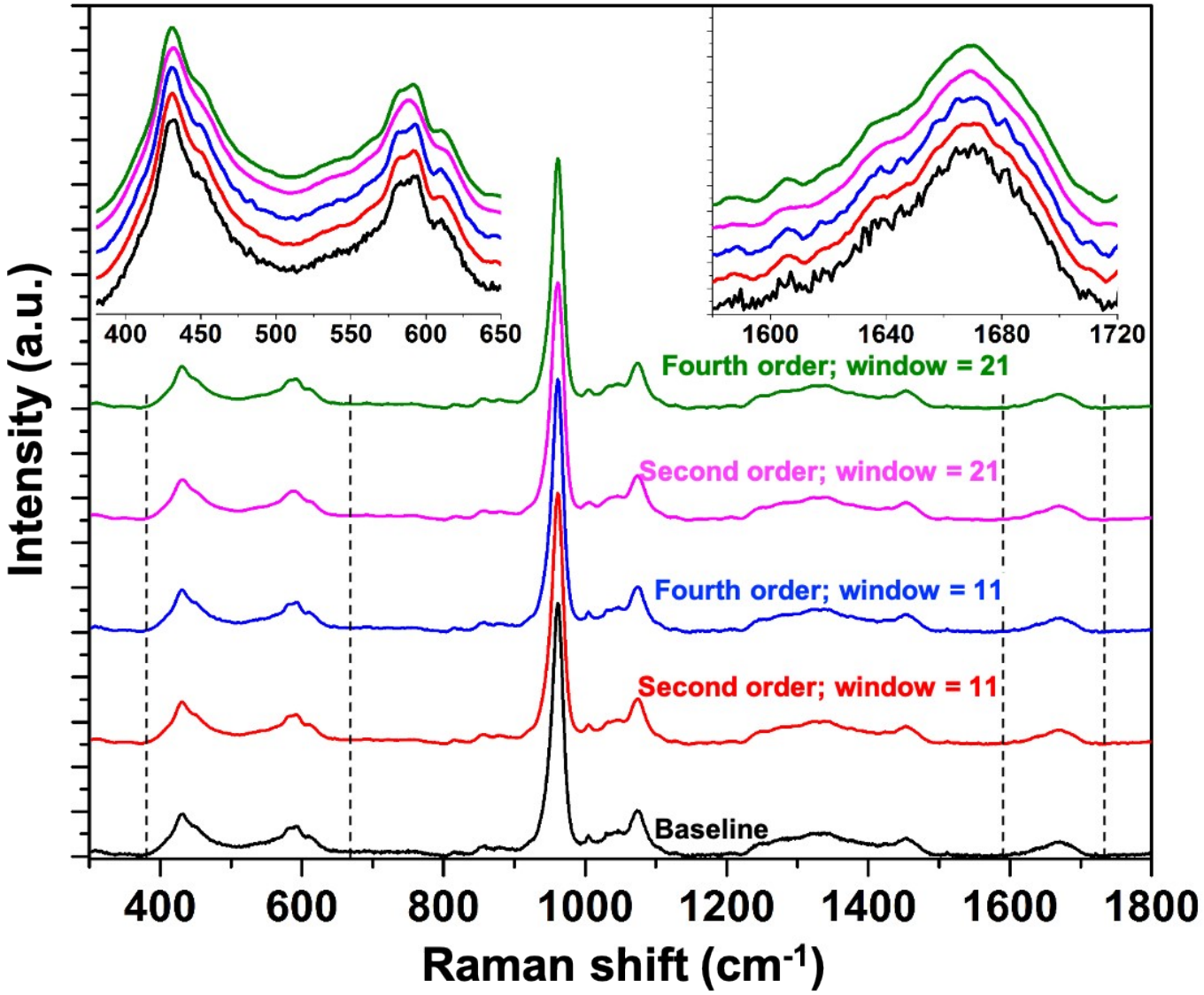

Figure S11: Effects of the order of the polynomial curve and the window size on 'smoothing' the Raman spectrum of bone. For a given order, doubling the size of the window that dictates the range of the polynomial fit makes for a smoother, less noisy spectrum at the risk of losing subtle peaks. A fourth order polynomial better preserves the original signals than a second order polynomial when using a smaller window size. The digital filtering of the spectra in this example was done using OriginPro.

Table S1. p-values from repeated measure (filter and ratio method), three-way analysis of variance.

Property	Filter	Method	Age	Filter x Method	Filter x Age	Method x Age	Filter x Method x Age
v_1PO_4/Amide I	0.0002	<0.0001	<0.0001	0.0002	0.0672	<0.0001	0.0669
v_1PO_4/Pro or v_1PO_4/Pro+Hyp	<0.0001	<0.0001	<0.0001	<0.0001	0.2394	<0.0001	0.2514
v_2PO_4/Amide III	<0.0001	<0.0001	0.0003	<0.0001	0.9671	0.001	0.9598
v_1PO_4/CH_2-wag	0.0002	<0.0001	<0.0001	0.0002	0.8409	<0.0001	0.8181
CO_3/v_1PO_4	0.0007	<0.0001	<0.0001	0.0006	0.0502	0.0001	0.0401

Table S2. p-values from repeated measure (method and baseline), three-way analysis of variance (filtered spectra).

Property	Method	Baseline	Age	Method x Baseline	Method x Age	Baseline x Age	Method x Baseline x Age
Crystallinity	<0.0001	0.0006	<0.0001	0.9787	<0.0001	0.1210	0.6971

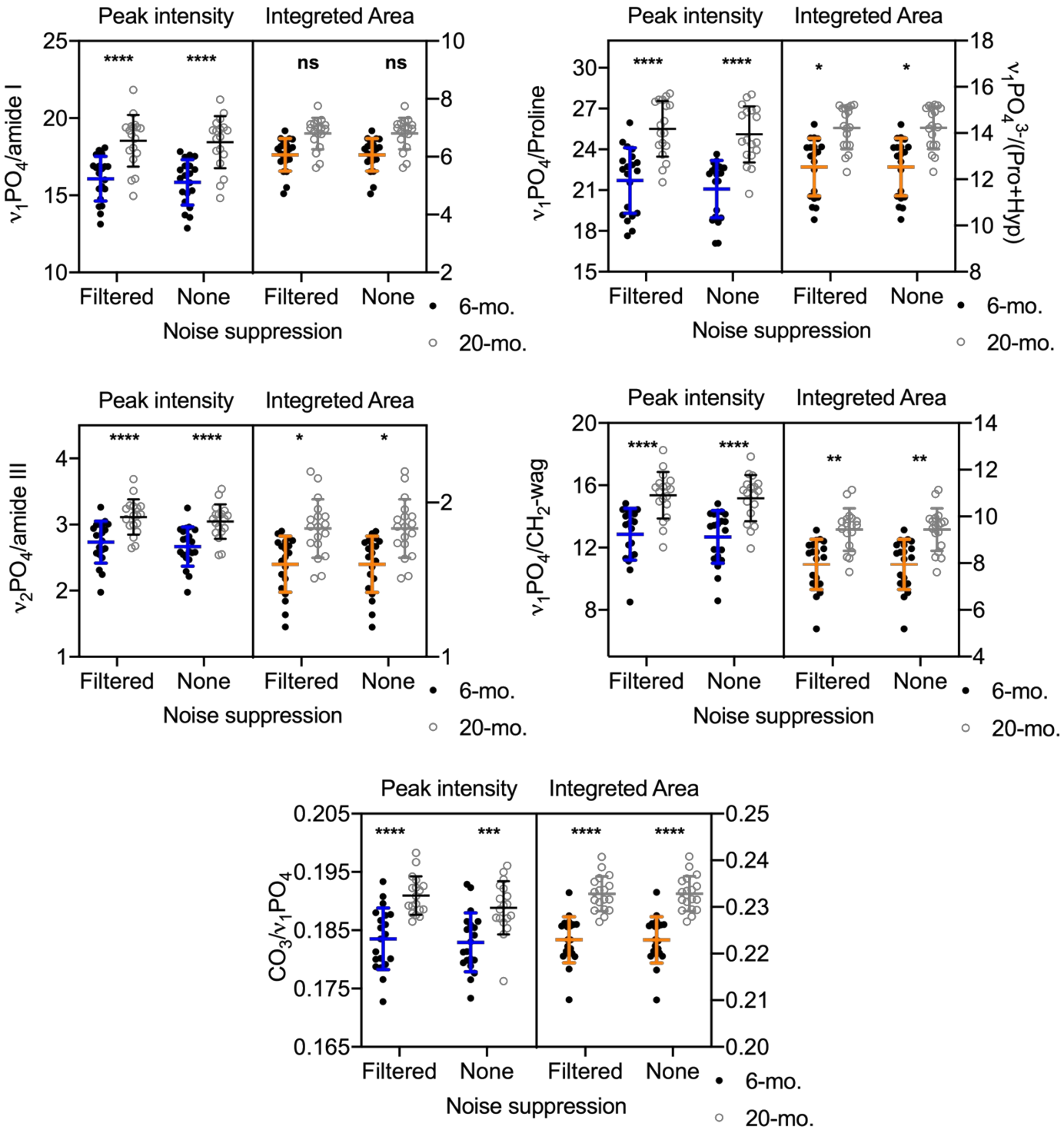

Figure S12: Effects of noise filtering and method of determining peak ratios on the age-related differences in mineral-to-matrix ratio and type B carbonate substitution. All peak ratios were higher in the old mice than in the young adult mice (mean±SD), regardless of noise suppression or method. The age-related difference in nu1 phosphate per amide I was not significant when determined using the integrated area method. Note however that p-values came from the post-hoc Tukey test of multiple pair-wise comparisons that maintains a family-wise level of confidence = 0.05. Without this adjustment, the difference for this peak ratio is significant (see Table 4).

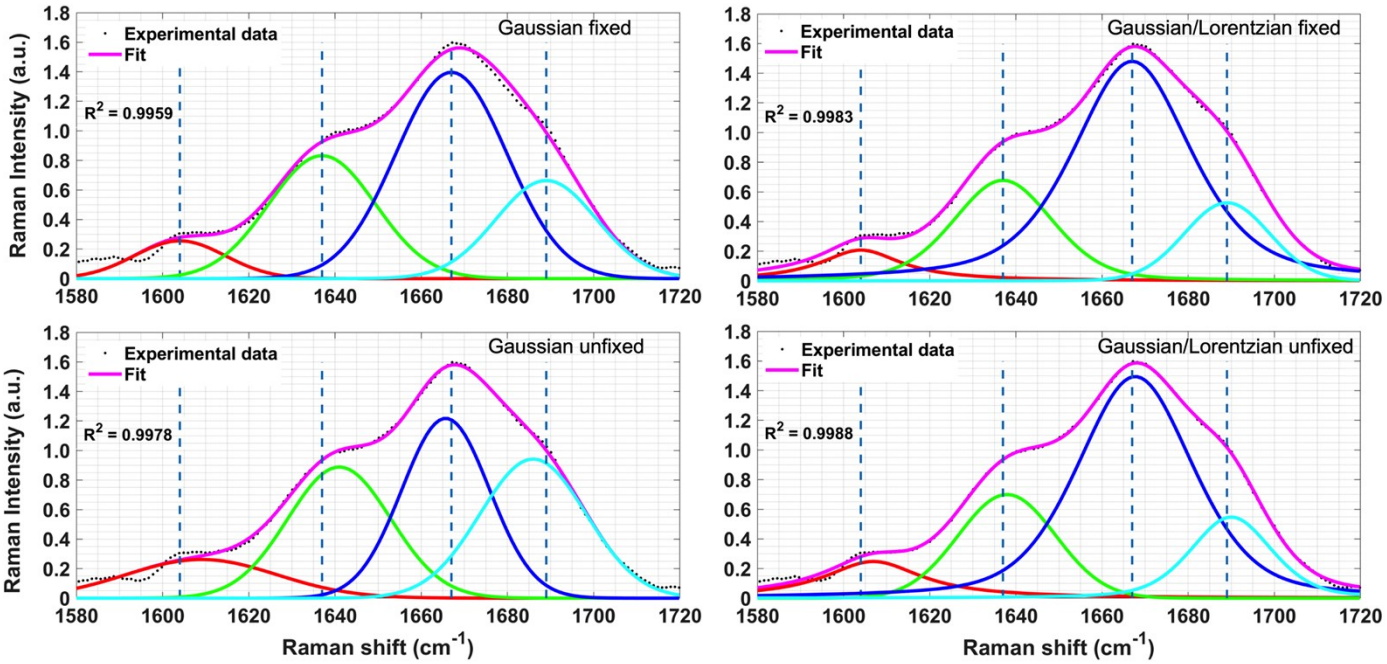

Figure S13: Deconvolution of the amide I band using 4 different methods (MATLAB). Excellent fits of 4 sub-bands to the same amide I band can be achieved whether the position of each band is fixed at the minima of the 2nd derivative spectrum (vertical dashed lines at 1605, 1638, 1667, and 1688 cm^{-1}) or unfixed such that each band can move within ±5 wavenumbers of the fixed positions and whether the sub-bands are 100% Gaussian or a blend of Gaussian and Lorentzian functions. The area and height of the sub-bands vary among the 4 deconvolution methods.

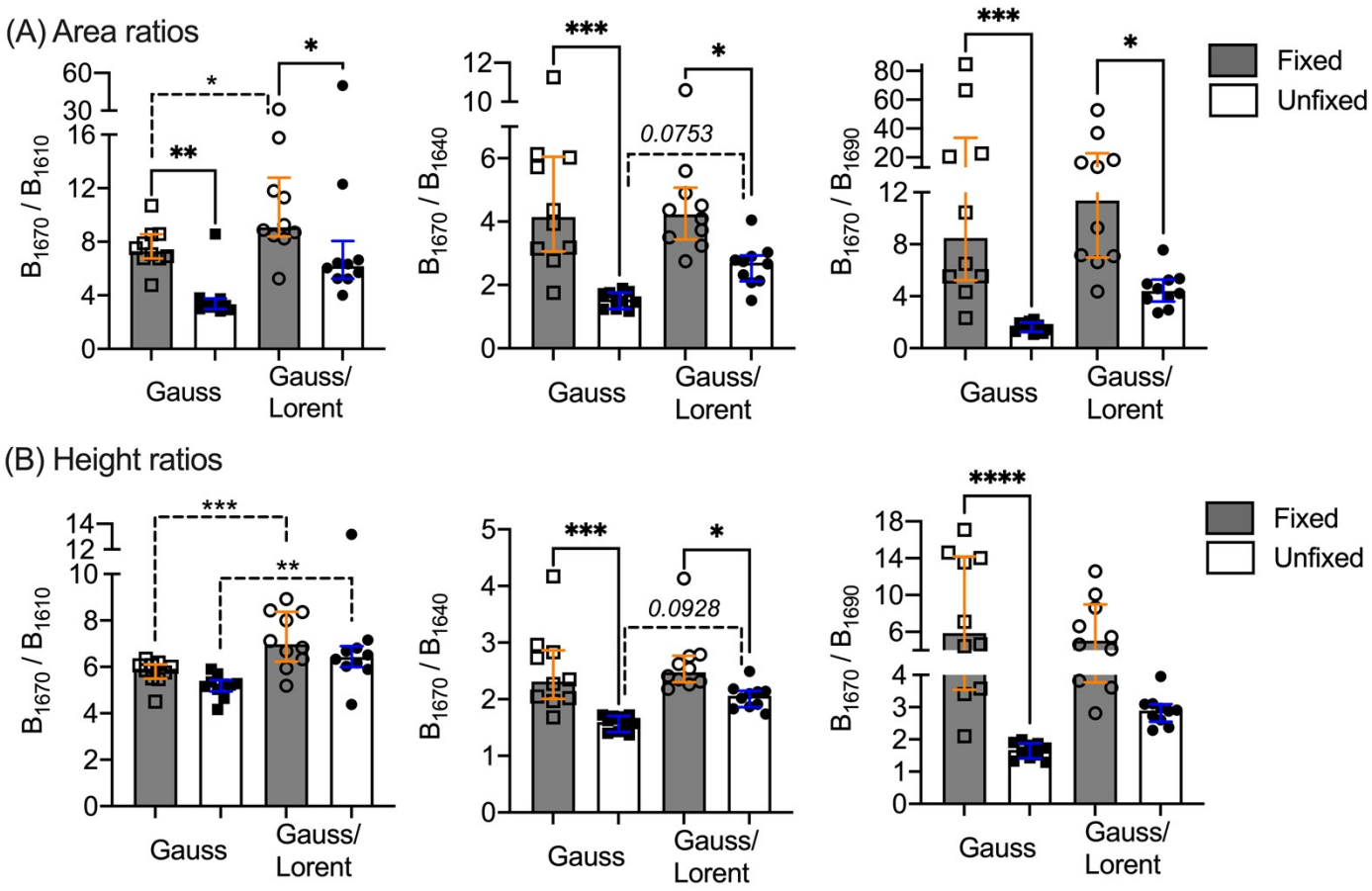

Figure S14: Varying sub-peak ratios among different deconvolution methods. When the position of each sub-band was allowed to move to lower or higher wavenumbers from the local minima of the 2nd derivative spectrum, amide I sub-peak ratios varied regardless of whether the area (A) or height (B) of the sub-bands was used in the determination. Sub-peak area and height ratios were higher when the positions of the sub-bands were unfixed than when they were fixed to the local minima. This was case for the fitting of 100% Gaussian curves and for the fitting of blends of Gaussian and Lorentzian functions (Gauss/Lorent). One exception was the height of sub-band at 1670 cm^{-1} per height of sub-band at 1610 cm^{-1} (B_{1670}/B_{1610}). The height ratio B_{1670}/B_{1610} also did not significantly vary between fixed and unfixed for the Gauss/Lorent fits. This blending of the 2 non-linear functions also resulted in higher sub-peak ratios compared to Gauss fits, regardless of the determination being based on area (A) or height (B) ratios, but significant differences were primarily observed for B_{1670}/B_{1610}. Note that the variance as depicted by the interquartile range in orange (Fixed) and in blue (Unfixed) was less when the positions of the sub-bands were allowed to move (Unfixed). Within area ratios and height ratios, significant differences among the 4 groups (Gauss-Fixed, Gauss-Unfixed, Gauss/Lorent-Fixed, and Gauss/Lorent-Unfixed) were determined using the non-parametric Friedman test. Since the test indicated that all sub-peak ratios depended on group, Dunn's multiple comparisons test determined whether Fixed was different than Unfixed within deconvolution method (Gauss and Gauss/Lorent) or determined whether Gauss was different than Gauss/Lorent within each position case (Fixed and Unfixed). In other words, p-values were adjusted for 2 separate pair-wise comparisons with a family-wise confidence level = 0.05. The bars indicate the median.

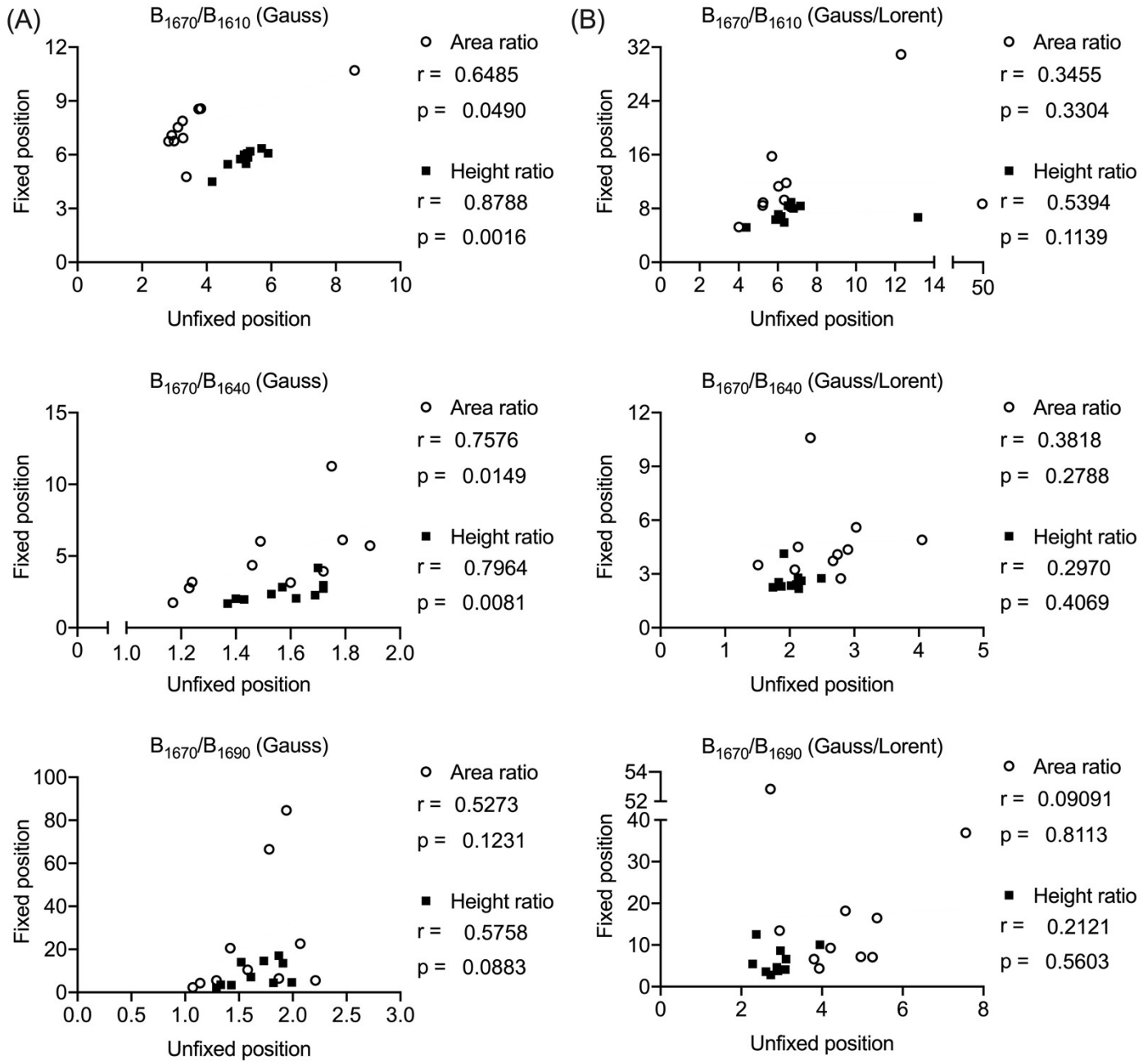

Figure S15: Sub-peak ratio correlations between fixed and unfixed positions. When the sub-bands were 100% Gaussian curves, 2 of 3 sub-peak ratios were correlated between fixed and unfixed positions (A). However, when the sub-bands were blend of Gaussian and Lorentzian functions, sub-peak ratios based on fixed positions did not correlate with their corresponding ratio based unfixed positions (B). The ability to find differences between any 2 experimental group will depend on the selected deconvolution method. P-value is provided for each Spearman's correlation coefficient (r).

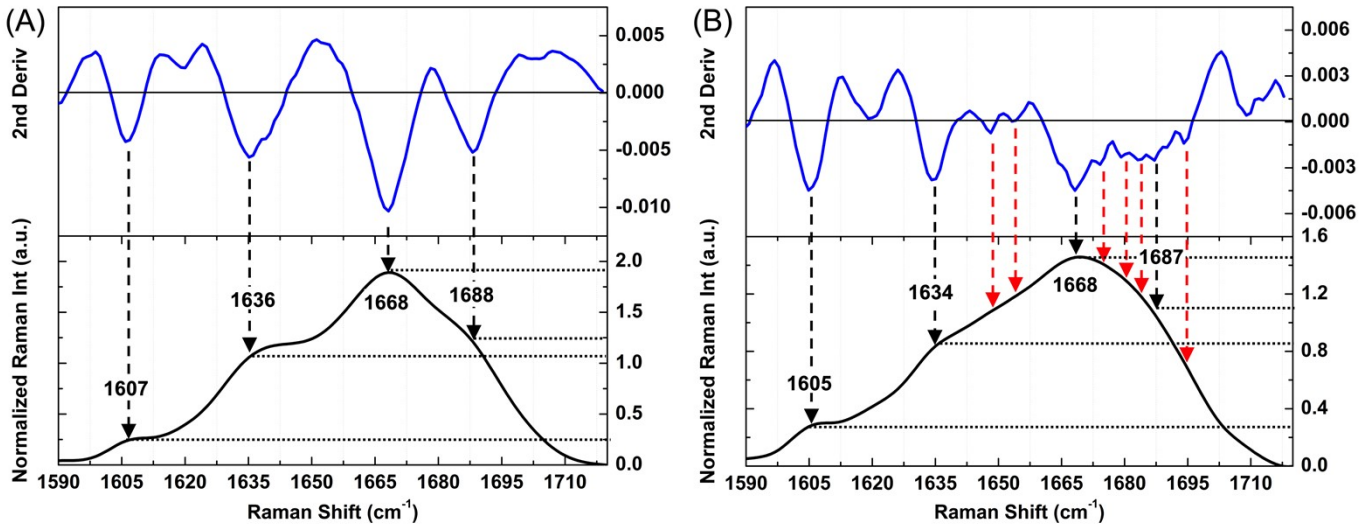

Figure S16: Determining sub-peak position before and after thermally treating bone. While the 2nd derivative spectrum (top left blue) of the pre-treatment amide I band (bottom left black) indicates 4 sub-peaks (A), the 2nd derivative spectrum (top right blue) of the post-treatment amide I band (bottom right black) indicates 10 sub-peaks. Horizontal dotted lines show the corresponding peak intensities at the wavenumbers that matched across the pre- and post-treatment spectra. Successively baking the bone samples at 110 °C, 120 °C, 130°C, and at 140 °C caused additional sub-peaks (red dashed arrows). See Nyman et al. JBMR Plus. 2019 for details on the baking treatment.

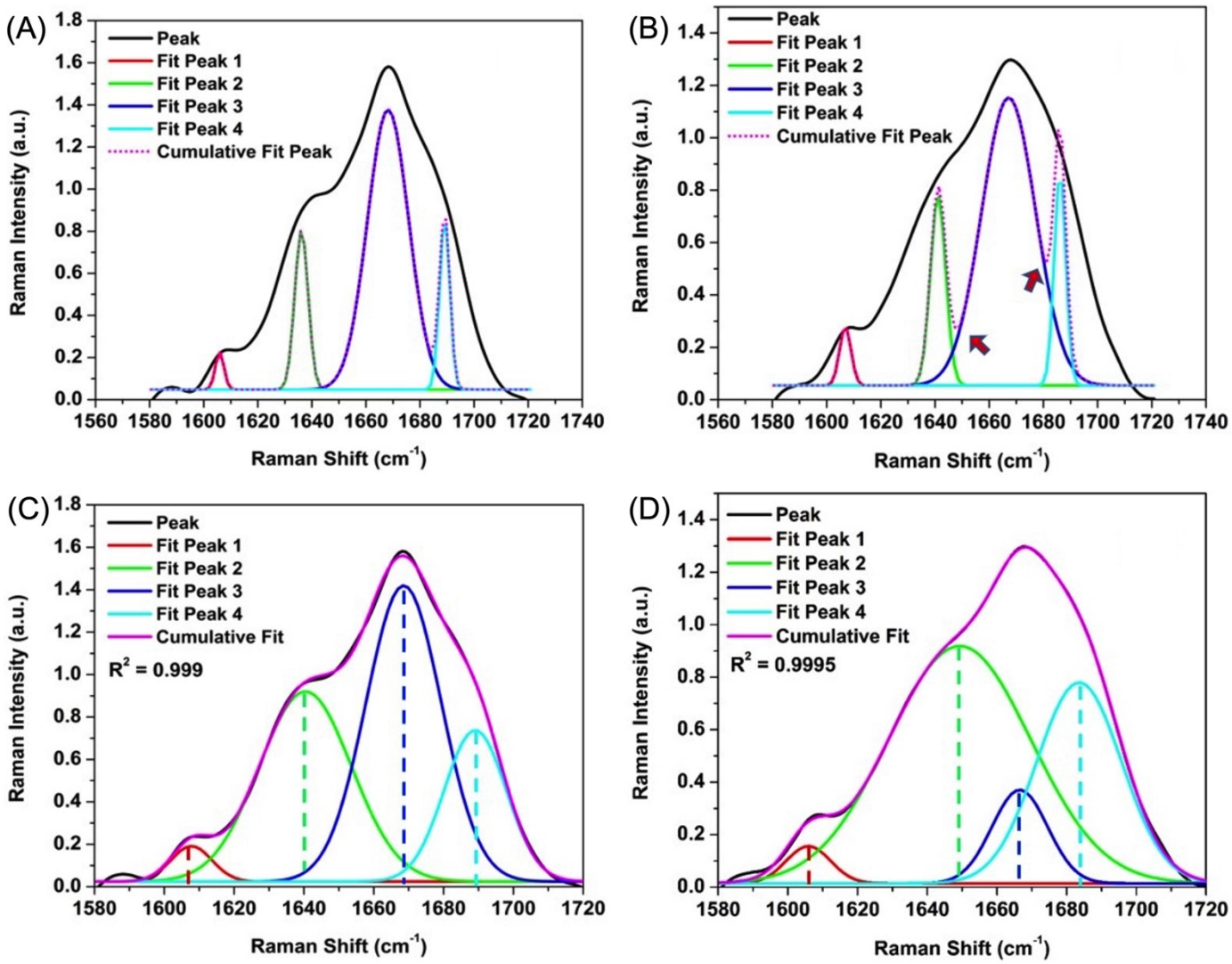

Figure S17: Fitting process by deconvolution using 100% Gaussian curves. Sub-bands are centered at local minima of the 2nd derivate spectrum of the pre-treatment (A) and post-thermal treatment amide I band (B). The height and width of each sub-band is varied per iteration until the convergence fit is achieved (C-D). The initial cumulative fit at ~1650 cm^{-1} and at ~1680 cm^{-1} is elevated (arrows) because of overlapping of sub-bands. As a result, the deconvolution of post-treatment amide I band (D) is different from the deconvolution of post-treatment amide I band (C).

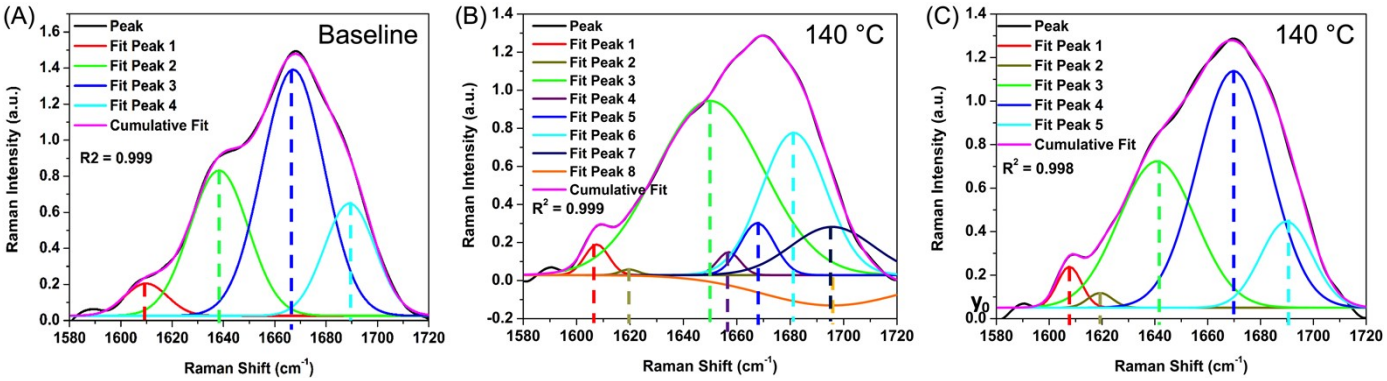

Figure S18: Comparison of deconvolution between pre-treatment amide I band and post-thermal treated amide I band. Four non-linear Gaussian curves that were unfixed to the local minima of 2nd derivative spectrum of the pre-treatment spectrum converged to solution with the highest sub-peak occurring at ~1670 cm^{-1} (A). In the case of post-treatment amide I band, additional sub peaks emerged causing a non-sensical fit of all the unfixed non-linear Gaussian curves (B). When optimization parameters, namely fixed bases to a y_0-offset and the inclusion of sub-bands with heights greater than 0.1 the maximum height among all sub-bands, the deconvolution is similar to the deconvolution of the pre-treatment amide I band (Baseline in A), though there an additional sub-band at ~1620 cm^{-1} (C).

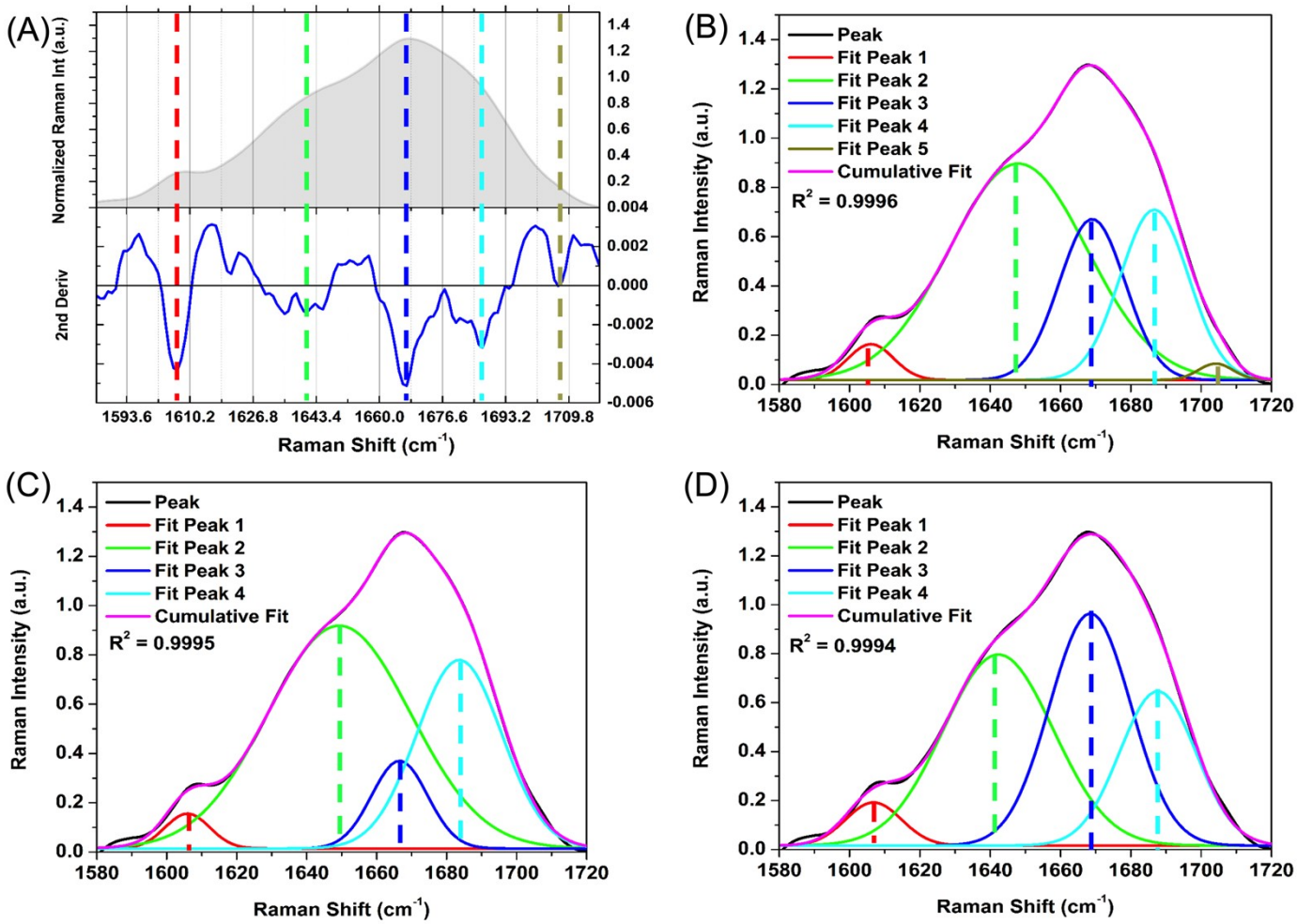

Figure S19: Deconvolution of the same post-treatment amide I band using three different optimization parameters. Local minima of the 2nd derivative spectrum indicated multiple peaks and so the ones included in the final deconvolution were labeled with vertical lines (A). 5 sub-peaks were used for convergence fitting (B). 4 sub-peaks also led to convergence fitting (C), however, notice that sub-peak around 1670 cm^{-1} is suppressed in both B and C. Fixing the initial estimated area of 1670 cm^{-1} resulted in correct sub-peak shapes (D).